EFDA–JET–PR(10)40

T.W. Versloot, P.C. de Vries, C. Giroud, M. Brix, M. G. von Hellermann, P.J. Lomas, D. Moulton, M. O' Mullane, I.M. Nunes, A. Salmi, T. Tala, I Voitsekhovich, K-D Zastrow and JET EFDA contributors

Momentum Losses by Charge Exchange with Neutral Particles in H-Mode Discharges at JET

Momentum Losses by Charge Exchange with Neutral Particles in H-mode Discharges at JET

T.W. Versloot[1], P.C. de Vries[1], C. Giroud[2], M. Brix[2], M. G. von Hellermann[1], P.J. Lomas[2], D. Moulton[3], M. O' Mullane[4], I.M. Nunes[5], A. Salmi[6], T. Tala[7], I. Voitsekhovich[2], K-D Zastrow[2] and JET EFDA contributors*

JET-EFDA, Culham Science Centre, OX14 3DB, Abingdon, UK

[1]FOM Institute Rijnhuizen, Association EURATOM-FOM, Nieuwegein, the Netherlands
[2]EURATOM-CCFE Fusion Association, Culham Science Centre, OX14 3DB, Abingdon, OXON, UK
[3]Imperial College of Science, Technology and Medicine, London, UK
[4]Department of Physics and Applied Physics, University of Strathclyde, Glasgow, G4 0NG, UK
[5]Association EURATOM-IST, Instituto de Plasmas e Fusão Nuclear - Laboratório Associado, IST, Lisboa, Portugal
[6]Association EURAROM-Tekes, HUT, P.O. Box 4100, 02015 TKK, Finland
[7]Association EURATOM-Tekes VTT, P.O. Box 1000, 02044 VTT, Finland
** See annex of F. Romanelli et al, "Overview of JET Results", (23rd IAEA Fusion Energy Conference, Daejon, Republic of Korea (2010)).*

Preprint of Paper to be submitted for publication in
Plasma Physics and Controlled Fusion

ABSTRACT.
The effect of a neutral density background on the toroidal angular momentum and kinetic energy profiles has been investigated in JET. Under equivalent conditions but with increasing gas fuelling during the flat top phase, it has been observed that both the edge rotation and temperature decrease. The increase in electron density was not sufficient to compensate the rotation and temperature loss such that both energy and momentum confinement times are significantly reduced. The ELM behaviour is observed to be significantly affected by the increased neutral influx. A simple 1.5D fluid model has been used to qualitative capture the neutral transport response within the plasma, followed by a forward model of the passive charge-exchange emission of carbon to obtain a corrected radial neutral density profile. It has been found that the neutral density reduces sharply over the edge region, with similar edge magnitudes in both the non-fuelled (Γ_0/n_e~1.2ms^{-1}) and maximum fuelled case (Γ_0/n_e~2.5ms^{-1}). Discharges with reversed-B operation exhibited even higher normalised neutral fluxes related to first orbit effects and increased wall interactions. Over the full neutral influx range, a decrease in pedestal thermal mach number from 0.25 to 0.14 was observed. Large neutral penetration up to the pedestal top (r/a~0.9) due to multiple charge-exchange interactions is obtained from the interpretive model. Under these multiple neutral-ion interactions, the impact on their associated losses are much larger for angular momentum compared to the thermal energy. The drag torque was seen to increase up to 10% of the total input torque, while energy losses appeared to be smaller. The magnitude of this sink by neutrals was comparable to torque required (30-50%) to explain the discrepancy between the energy and momentum confinement.

1. INTRODUCTION

The effect of plasma rotation on plasma confinement and stability has been an area of extensive research in recent years [1]. Early theoretical explorations into the role of plasma rotation [2,3] have led to a wide range of experiments into momentum transport on several devices [4,5,6,7]. For example, results in [8] show that a radial rotation gradient can play a role in the suppression of turbulent ITG dominated transport [9]. This naturally raises the question how to generate sufficient angular momentum and what determines its radial profile. It is clear from experiments [10,11] that the transport of momentum and energy is not necessarily similar while at the same time it remains partly unknown which processes contribute in driving angular momentum. Due to the existence of an inwards convective pinch velocity [7,12], the magnitude of the edge rotation is found to contribute significantly to the global momentum profile due to the large pinch velocity (RV_p/χ_ϕ~4-10) in typical modelled JET H-mode cases [13]. The observed core rotation gradient is therefore both related to the external torque flux as well as the absolute magnitude of the momentum density, in particular at the plasma edge. Hence, in order to accurately predict the observed rotation profile, a better understanding of the processes that influence the local edge momentum density is required.

Several effects contribute in determining the edge momentum. In JET, the dominant source of torque is provided by Neutral Beam Injection (NBI). The particle beam are injected in the co-

current direction and due to beam attenuation and the trapping of fast particles, most of the torque is deposited off-axis [14]. Non-ambipolar losses of fast particles due to Toroidal Field Ripple [13] or Resonant Magnetic Perturbations [15] can provide a source of counter-current directed torque. The ripple magnitude during normal operation at JET is however small (δ_{ripple}~0.08%) and the associated torque is considered negligible in this case, even at the plasma edge. Other sources such as intrinsic rotation and residual stress might also be present, although these are typically orders of magnitude smaller than NBI driven torque [1]. The dominant loss of momentum takes place at the boundary of the plasma by flows to the stationary wall. With the presence of Edge Localised Modes (ELMs), the repetitive collapses of the H-mode pedestal also cause an ejection of both energy and momentum [16]. The steady-state momentum density at the edge, $l_\varphi = n_i m_i R v_\varphi$, is thus the result of the interplay between sources and sinks with radial transport from the core by diffusion and local inwards convection.

An additional process at the edge is the presence of neutral particles which is known to be an efficient sink of angular momentum [17]. The penetration of neutrals from the plasma boundary causes a loss of both energy and momentum by Charge-eXchange (CX) interactions with the main plasma ions. In fact, the mechanism of neutral penetration has been studied in relationship to characteristic pedestal properties (width and heigh) [18] as well as its connection to the L-H transition [19]. In both cases, the presence of atomic physic effects at the plasma boundary could provide an insight in global plasma properties due to external, usually relatively uncontrolled conditions like recycling and conditioning of plasma-facing components. However, as of present no atomic physics components have been directly identified in the energy confinement time scaling, although hints of missing parameters could point in the direction of boundary effects [20]. In typical tokamak experiments, the ionisation frequency is slower than the charge-exchange frequency. This process is critical to the extent that it can greatly enhance the penetration depth due to multiple CX interactions before impact ionisation [21]. At each interaction, a neutral and plasma ion exchange identity, but as the momenta of both are uncorrelated, this results in large-angle scattering where new born neutrals carry away the original ion momentum and energy. These neutrals thus show a random walk process where parts of the original ion angular momentum can now easily be lost by viscous dissipation [21]. Interesting to note is that such conversion of rotational energy to thermal energy can also also cause local heating [22] which could be related to generating poloidal flows. The penetration of neutrals is therefore expected to have a different impact on the momentum and energy balance.

Unfortunately, the characterisation of atomic physics at the edge and in particular the neutral density background, remains difficult to quantify directly in experiments due to the inherent complex atomic processes involved. The neutral density profile therefore remains one of the least well diagnostic fusion plasma properties, with usually only indirect measurements available. Recent progress in multi-dimensional edge models have begun to uncover the spatial distribution of neutrals from highly localised sources [23,24]. For example, results from [25] show that during gas fuelling

close to the X-point region, the neutral density is highly peaked in the divertor region from the LCFS outwards, while at the pedestal region no strong poloidal variation was found. This could thus allow for a simpler 1.5D neutral fluid approximation to model the neutral transport response of the plasma within the LCFS. The approach presented here in this paper has been to qualitatively capture the atomic physics related to multiple neutral-ion interactions using a 1.5D neutral fluid code. The uncalibrated neutral density is then used to forward model the passive charge-exchange emission profile [26] and subsequently compared to the line integrated intensities measured by the Charge Exchange Recombination Spectroscopy (CXRS) diagnostic [27]. This approach allows for a correction on the neutral density obtained from the model. The final goal of this paper is to compute the magnitude of momentum and energy losses due to charge-exchange processes at the plasma edge. The presence of additional momentum losses due to increases neutral interactions could help in explaining the variations in confinement time ratio ($R_\tau = \tau_E/\tau_\varphi$) and the observed range in thermal mach number [10].

This paper is build up as follows; In the next section, the observations on global and edge parameters during several JET H-mode plasmas with varying levels of external gas fuelling are presented. Large variations in the observed D_α emission, a measure of the neutral density, are observed. Changes in profiles of angular frequency ($\omega = v_\phi/R$), temperature (T_i,T_e) and electron density (n_e) are shown here. The method used to calculate the neutral density (n_0) in combination with the validation technique employed is discussed in section 3. The relevant neutral particle dynamics are discussed. In section 4, the estimated magnitude and spatial distribution of the charge-exchange associated losses are presented, taking into account the penetration by multiple charge-exchange interaction processes. Conclusions are presented in the last section and discussed with an outlook on future work in this field.

2. EXPERIMENTS

To investigate the influence of a neutral particle background on the main plasma, a series of discharges was selected with similar plasma configurations and equal external heating power, but increasing input gas flux during the flat top H-mode phase. Heating was predominantly supplied by the NBI with $P_{TOT} = 15(\pm1)$MW and a resulting total torque input of $T_{NBI} = 16(\pm1)$Nm. The gas influx (Γ_0 in elec/s) was supplied by toroidal ring valves located at the inner divertor and increased from 0 (non-fuelled) to $\Gamma_{0,max} \sim 4\times10^{22}$ elec/s. The plasma configuration used is a high triangularity ($\delta \sim 0.40-0.44$) type-I ELMy H-mode with a plasma current of $I_p = 2.5$MA and toroidal field of $B_T = 2.7$T. The presence of an external gas flux has a significant impact on the plasma behaviour as can be seen in figure 1. A regular ELM period (f_{ELM}~10Hz) is observed in the non-fuelled case, while with increasing fuelling the ELM behaviour becomes less pronounce with an overall increase in ELM frequency and the baseline D_α-radiation from a vertical line of sight on the outboard side. This is consistent with the general observations of plasma fuelling. A higher fuelling rate however does not necessarily result in a larger neutral density near the plasma due to vessel pumping and/

or the plasma shape. The increase in visible emission along different viewing lines is nevertheless an indication of a higher neutral background poloidally around the entire plasma even though the input valve was localised in the divertor region in these cases. A higher edge electron density is thus observed with higher fuelling as also generally observed and studied in detail in e.g Ref. [28]. With plasma velocity measurements from the CXRS diagnostic, the thermal angular momentum density ($l_\varphi = n_i m R v_\varphi$) profile is calculated as shown in figure 2a. The ion species measured is that of the main impurity ion, C^{6+}, and it assumed here that all the ion species are in equilibrium such that the bulk plasma ion temperature and velocity can be computed. A decrease in l_φ over the full profile is observed, which seems to originate mainly from a reduction at the pedestal as core transport is not assumed to be effected significantly. Both ion temperature and rotation velocity are observed to decrease as the electron density increases during the gas scan, but also the ion pressure at the edge is seen to decrease. The overall result is a drop in confinement quality with neutral influx which is in agreement with earlier observations in several devices [20,29,30], although not in all cases necessarily directly linked to the atomic physics related to possible increased neutral penetration. The induced changes in pedestal conditions can also alter the pedestal confinement as can be clearly seen in the ELM behaviour for various gas fuelled discharges in figure 1. In fact, gas fuelling beyond 4×10^{22} elec/s was not performed in this gas scan due to a significant decrease in confinement enhancement factor ($_{H98IPB(y,2)}$).

All effects combined, a decrease in the thermal mach number ($M_{th} = v_\varphi/v_{th}$) near the pedestal top (r/a~0.9) from approximately 0.3 to below 0.2 is obtained, as can be seen in figure 2a. The thermal Mach number is directly related to the ratio of kinetic to thermal energy and their confinement times [13]. In comparison to the non-fuelled case, the maximum fuelled discharges has a fraction of angular momentum of $L_{\varphi,max}/L_{\varphi,0} = 0.50(\pm0.07)$ compared to $W_{th,max}/W_{th,0} = 0.67(\pm0.08)$ for the total thermal energy (see also figure 5a). Both input power and torque deposition were remained constant throughout the gas scan, therefore the confinement times decrease significantly with their ratio (R_τ) increasing slightly with a decrease in M_{th} as also observed in [10] for a large set of JET discharges. This difference in the reduction of the momentum and energy density at the plasma edge suggests a discrepancy in the local losses. These could, albeit possibly partly, be attributed to the presence of neutral-ion interactions with a neutral background. Due to gas fuelling, both the neutral influx around the plasma periphery as well as the ion (and electron) density at the plasma edge increase, which further enhance the magnitude of charge-exchange losses. Additional losses by radiation, convection by parallel transport along field lines and changes in stability also have an influence on both τ_E and τ_φ, but these are not necessarily similar. Those processes are not further discussed and instead the focus in this paper has been in estimating the relative magnitude of the momentum and energy losses due to charge-exchange interactions with background neutrals.

3. NEUTRAL PARTICLE DYNAMICS

In general, high temperature and density plasmas are considered to be impermeable to neutrals

with a penetration depth limited to only a few cm ($\lambda_{MFP} = v_0/(n_e<\sigma v>_{CX})$, [20]). However, this does not necessarily result in a total absence of neutral particles within the main plasma as the charge-exchange frequency ($<\sigma v>_{CX} \sim 10^{-13-14} m^3 s^{-1}$) is typically much larger than the ionisation frequency ($<\sigma v>_{ionisation} \sim 10^{-15} m^3 s^{-1}$). At each CX interaction, a plasma ion and neutral 'swap' identity, allowing the now high energetic or hot neutral to penetrate deeper into the plasma, while the low energetic ion is confined by the magnetic field at the interaction location. As a result, a neutral background will be present due to constant penetration of low energetic or cold neutrals through the last closed flux surface although many orders of magnitude smaller than the electron density in the plasma core ($O(n_0) \sim 10^{11-12}\ m^{-3}$). The presence of neutral particles can therefore facilitate in redistributing energy, particles and momentum. In figure 3a, a schematic representation is shown of this multiple CX interaction process. An external cold neutral, n_{0c}, collides with a plasma ion, n_{ih}, exchanges charge and produces a hot neutral, n_{0h}, that scatters unidirectionally. This CX interaction can be considered as a soft interaction [31] where the outgoing neutral obtains a velocity characterised by the local ion temperature only. A fraction of the neutrals will penetrate deeper into the plasma and at a secondary interaction, the process repeats itself. Only in this case, the thermal energy, a scalar quantity, from the hot neutral is fully transferred back to the bulk plasma. The original ion angular momentum on the other hand was transferred to momentum of the neutral fluid, which is unbound by the magnetic field, and is therefore assumed completely lost to either the wall or by viscous dissipation [21,22]. The number of multiple interactions and mean free path between interactions can also be high considering the difference between ionisation and charge-exchange frequency. Multiple CX interactions can therefore result in a difference between the associated momentum and energy losses.

The magnitude of momentum losses by CX interactions is given by $T_{CX} = n_0 n_i m <\sigma v> CX (v_i - v_0)$ [32]. As can be seen, the magnitude is directly related to the spatial and velocity distribution of the neutral fluid. Additionally, the neutral fluid also consists of several energy components resulting from CX interactions (cold, hot) and also from e.g. fuelling and recycling. This and the fact that direct measurements of the neutral density are relatively complicated, necessitates the use of extensive modelling in order to quantify n_0. However, it has been shown that qualitatively describing the neutral transport response of the plasma using a 1.5D fluid approximation can give satisfactory results [25].

Here, we use a 1.5D cylindrical fluid code (FRANTIC [33,34]) to determine the radial neutral transport response of the plasma to an external neutral source. The neutral gas influx was characterised by two contributions with their relative intensities and average energies obtained from the visible Bremsstrahlung spectrum (n^0_{hot} [I = 0.35, E = 10eV], n_{0cold} [I = 0.65, E = 1eV]). Between discharges in the gas scan, these values were not observed to change much, although they could potentially vary widely depending on, among others, recycling and interactions with plasma facing materials. The neutral transport response and thus the shape of the neutral density profile are highly dependent on the edge profile of n_e and T_e. Therefore, high resolution Li-beam data was used in combination

with Thomson Scattering (TS) to obtain ELM averaged electron density profiles. The electron temperature is obtained from Electron Cyclotron Emission (ECE) and TS. The model results in a qualitative estimate of exponential n0-profile within the plasma, but is unable to directly quantify its absolute magnitude. Therefore, a following method was implemented in which the uncorrected neutral density from FRANTIC was used to forward model the passive charge-exchange (PCX) emission as also observed by the CXRS diagnostic. Each line-of-sight of the CXRS measures besides a local active signal from the intersection with the neutral beam also passive emission from the interaction between deuterium neutrals and impurity ions ($C^{6+} + D^0 > C^{5+*} + D^+$) along the line-of-sight. The carbon density is also obtained from the CXRS spectra after which an estimate on the total integrated photon flux can be made taking the appropriate atomic cross sections into account (see also [26]). This method then results in a linear adjustment factor needed to accurately quantify the n_0-profile.

Figure 3b shows the adjusted n0 and ne profiles for two discharges of the gas-scan. With increasing neutral influx, the electron density profile increases. This process actually shields the core plasma by reducing the penetration step size of neutrals. This shielding seems to partly balance the increased influx and it is found that in both cases the n_0-profile obtained is of similar order of magnitude at the plasma edge, $n_0(r/a{\sim}1.0) \sim O(10^{15\text{-}16})m^{-3}$. Also shown in figure 3b are corresponding results from independent 2D edge model calculations using EDGE2D-Eirene [35]. The poloidally averaged neutral density obtained with the PCX-corrected results from the fluid model agrees well with 2D model which gives confidence that the above method is able to quantify the neutral density roughly in the right order of magnitude. In figure 4a, the poloidal cross-section of the neutral density shows the spatial variation of the neutral density at the boundary with the largest concentration in the X-point region near the divertor. In this case, a low level of active external gas dosing was supplied. Variations of the neutral density of several orders of magnitude is clearly seen, as also shown in figure 4b as a function of poloidal angle for both a low fuelled and high fuelled case. The variation of the neutral density appears to be less strong within the separatrix, especially in the case of high fuelling as is also observed and discussed in [36]. This might be related to the relatively large flux expansion in the divertor region shielding the main plasma when fuelling in the divertor region. The poloidal asymmetry due to local sources indeed results in large increase in values for the flux expansion parameter discussed in [18] from the separatrix outwards. Nevertheless, large uncertainties will remain on the accuracy (in the order of magnitude) of the neutral density at the pedestal due to the lack of direct experimental verification.

4. MOMENTUM AND ENERGY LOSSES

Using the derived neutral density profiles, the charge-exchange associated frictional torque and power loss can be calculated. It must be noted that here we focus solely on the effect on angular momentum and do not include additional effects resulting from an increased neutral background, e.g. pedestal stability. Due to the increase in edge n_e the beam deposited torque and power calculated by an orbit

following Monte-Carlo code (ASCOT [37]) have shifted slightly outwards as shown in figure 5a. The magnitude of CX losses is concentrated dominantly at the edge, where the concentration is highest and quickly falls off as the neutral density decreases exponentially inwards. Nevertheless, a penetration up to the pedestal top (r/a~0.9) is obtained for the torque loss while the power losses appear more confined to the outer edge, which is in agreement with results obtained in [36]. In the case of additional fuelling, the magnitude of TCX increases more significantly in the pedestal gradient region. However, the penetration depth is not altered notably. As described earlier, a possible explanation could be related to the balancing of the increased influx with the higher shielding by the core plasma. Interesting to note is that even without applied fuelling, significant friction from the natural present neutral background is modelled. In both cases, the absolute magnitude of the CX losses is similar to the local beam torque deposition at the edge. The beam source includes both collisional and J×B generated torque. Although dominantly a torque source, CX interactions between beam neutrals (nb) and plasma ions can cause additional edge losses. Estimates of their magnitude showed however only a small contribution. As these losses do not depend on the neutral background and the nb flux was kept similar, these contributions were not included in this analysis.

The total loss due to CX interactions with background neutrals can now be calculated by volume integration, as shown in figure 5b along with the normalised values of W_{th} and L_φ. Due to the uncertainty in the diagnostic profiles at the edge, this has been done up to r/a~0.95. As discussed in Section 2, a general decrease in both W_{th} and L_φ is seen with increasing neutral influx. The neutral influx per unit area has here been normalised to the average electron density which is thus related to the number of neutrals per plasma unit charge (Γ_0/n_e [ms^{-1}]). For all gas-scan discharges, the frictional drag is considerably larger than the power losses and approaching up to 10% of the total input torque ($T_{CX}/T_\varphi \sim 0.10$) with $W_{CX}/P_{tot} < 0.03$. This results in a total CX drag of the order of 1.0-1.5Nm. This is consistent with the observation of the faster decrease in L_φ in comparison to W_{th}. The presence of CX losses however can not directly explain the general decrease in confinement times observed, which is most likely caused by secondary and indirect effects from fuelling on the plasma confinement. Nevertheless, the presence of neutrals at the edge is able to manifest itself as a significant sink of angular momentum.

5. CO- AND COUNTER ROTATION

Besides active gas fuelling, part of the neutral flux through the separatrix will result from recycled particles of the plasma-facing components. As was already seen in figure 4, this can already dominate the deuterium particle source. By now selecting similar discharges used in the gas-scan but with a large natural fraction of recycling, we can investigate higher neutral fluxes. Additionally, scattering of e.g. first orbit losses hitting the wall can result in relatively high energetic neutrals that are able to penetrate deeper into the plasma. Large amounts of orbit losses have been observed in JET under operation with reversed-B and counter-current NBI [10]. In figure 6a, two time-traces are shown of similar discharges in co-current (CO-NBI) and counter-current (CNT-NBI) at $B_T = 2.4T$ and

$I_p = 2.0$MA. In the case of CNT-NBI is can be clearly seen that the neutral background increases due to large increase in Dα-emission. Both the low- and high-energetic neutral populations increase. In this case even, the hot neutral component becomes of similar size as the entire neutral population in the CO-NBI comparison. The largest difference is however seen in a dramatic increase in the cold neutral component, which can be identified experimentally by the visible glowing of the limiter tiles. The rotation profile in the CNT-NBI discharges is in that case significantly reduced in comparison to the CO-NBI case with also a reduction in edge stead-state Mth. Interesting to note is that the Mth profile itself also changes in the core of the plasma with the gradient flattening as the neutral influx increases. This is most likely related to the magnitude of the pedestal as no significant transport differences in core transport were found in these discharges.

Determining the neutral density profile with the method presented in this paper, resulted in similar order of magnitudes of n_0 at the plasma edge. However in the case of CNT-NBI the electron density was on average lower in comparison. This combined results in much larger values of Γ_0/n_e. The beam deposition and associated CX losses are shown in figure 6b. In the case of CNT-NBI, the outwards directed orbit effects are seen to have shifted the torque deposition towards the outer parts of the plasma. Subsequently this greatly reduces the core torque flux, thereby reducing the core rotation gradient. The torque losses significantly increase when switching to CNT-NBI. With the beam torque deposition near the plasma edge, efficient losses not limited to only neutrals would now be able to result in fast momentum losses thereby preventing the rotation profile to develop. As was seen before, the power losses by CX-interactions increase similarly to the torque losses but remain localised further away at the boundary. This is seen also experimentally in relatively higher temperatures (T_e and T_i) in the pedestal region. At least in the CO-NBI cases, the presence of first orbit losses can result in a displacement current generating counter torque which contributes directly in lowering the edge rotation. When applying CNT-NBI, the generated torque will be in the opposite direction and equal in sign to the NBI driven torque at JET due to operation at equal helicity.

With an increasing neutral influx, the magnitude of the edge velocity is reduced resulting in a relatively larger momentum loss in comparison to the thermal energy. In figure 7a, the edge M_{th} is shown as a function of normalised neutral influx for all discharges used in this paper. It is clearly seen that with increasing neutral influx the Mach number reduces where the lowest value was obtained during counter-current NBI. Interesting to note here is the location of a counter-current NBI discharge at the lowest value of Γ_0/n_e. This discharge was performed under similar conditions, but with an increased radial clearance on the low field side, $\Delta_{wall} = \Delta_{wall} + 5$cm. This effectively puts part of the neutral source further away from the core plasma with possibly a wider scrape-off layer in between the edge and plasma-facing materials. Improved performance has been obtained by plasma shaping in JET [38]. Further investigations into the influence of wall clearance as well as plasma shape (elongation, triangularity) is needed to investigate these effects as they can have a large effect on the magnitude of the neutral background.

Unfortunately, the uncertainty on the absolute magnitude of the CX losses remains large due to

limited diagnostic coverage and the inherent complexity of the spatial distributed atomic physics processes. To independently check the validity of the required magnitude, we can compare the CX associated torque to an empirical missing torque by assuming $\Delta T = T_\varphi - L_\varphi/\tau_E$, where L_φ/τ_E is the global required torque under the assumption of equal confinement times. The result is shown in figure 7b where most of the model results are seen to agree between a factor of 2 to 3 with the required loss. It has to be bore in mind that no distinction between different torque losses is made here. Additionally, the confinement times are not necessary identical as shown in the first section of this paper. Never the less a fraction of up to 50% does make the relatively crude model assumptions plausible and more importantly would suggest that neutral friction plays a dominant role in the discrepancy between the momentum and energy confinement time.

CONCLUSIONS

It is observed that the stored angular momentum and thermal energy content decrease with increasing gas dosing in typical JET H-mode discharges. The angular momentum is however more greatly affected with a significant lowering of the thermal Mach number at the edge. Due to multiple charge-exchange interactions within the lifetime of a neutral particle, additional angular momentum can be lost. This could explain the imbalance observed between the energy and momentum losses. An increase in friction losses up to 10% of the total input torque was calculated using a neutral transport response model. The CX power losses appeared smaller and localised mostly at the boundary while torque losses were able to penetrate further inwards (r/a~0.9). The largest neutral flux was found in the case of counter-current NBI ($\Gamma_0/n_e \sim 5 ms^{-1}$) which also showed the lowest edge M_{th}~0.12 and a large decrease of the rotation profile over the full plasma radius. The uncertainty on the absolute magnitude of the CX losses remains large, although its magnitude was found comparable with the required missing torque (figure 7b).

A neutral background, unbound by the magnetic field, is an inherent non-symmetric source of particles. More detailed edge diagnostic data in combination with 2D neutral transport calculations are therefore required to fully quantify the spatial distribution of the CX associated losses. Initial 2D model results [35] show a large poloidal variation in neutral density of several orders outside of the separatrix with the highest density in the divertor region. However, field flux expansion could play a key role, reducing the penetration depth and influence in the divertor region while increasing penetration depth in regions of high neutral density in the main chamber. Additionally, particles following closed field lines might spend more time in these high density regions. Full 3D orbit following codes will be required to investigate these effects [23, 24]. Nevertheless, average neutral densities at the plasma edge in the order of $10^{15\text{-}16}$ m^{-3} are found in agreement with a PCX collisional radiative model. With significant torque input by NBI (>16Nm) these levels are already high enough to cause a significant drag in the edge of a fusion plasma.

It must be noted that in this analysis only the effect of neutral particles by neutral-ion charge-exchange processes has been investigated. Other losses and transport processes which could effect

the momentum pedestal and confinement have been excluded. Currently, several edge models discuss a direct influence of neutrals in the formation of the H-mode pedestal and indeed a significant influence on the confinement quality during a gas-scan has been observed in this study. Magnetic perturbations and orbit losses could also lead to an imbalance between momentum and energy losses, although these effects will also play a role in the development of the neutral background due to increased particle interactions with the wall. An accurate treatment of the neutral pressure therefore requires all these effects to be included self-consistently.

Concluding, a neutral background can have a large impact on the boundary value of the rotation. A lower neutral hydrogen background, as expected in the upcoming ITER-Like Wall experiments in JET, would have a beneficial effect of reducing the neutral friction and raising the edge rotation. This will have an indirect effect on the core gradient due to the presence of inwards convective transport. This is similar to the behaviour observed when applying Toroidal Field ripple [13]. Equivalent to here, a lowering of the edge momentum resulted in a reduction of the observed core rotation gradient. The presence of atomic physics at the edge can therefore play a direct role in setting the necessary boundary conditions for core transport and needs to be taken into account when predicting both global and core plasma properties.

ACKNOWLEDGMENTS

The authors would like to thank W. Goedheer and D.C Schram for helpful discussions and guidance. This work, supported by the European Communities under the contract of Association between EURATOM and FOM and CCFE, was carried out within the framework of the European Fusion Development Agreement. The views and opinions expressed herein do not necessarily reflect those of the European Commission.

REFERENCES

[1]. deGrassie J.S. 2009 Plasma Physics and Controlled Fusion **51** 124047
[2]. Garofalo A.M. et al 2001 Nuclear Fusion **41** 1171
[3]. Burell K.H. 1997 Physics of Plasmas **4** 1499
[4]. Solomon W.M. et al 2009 Nuclear Fusion **49** 085005
[5]. Nishijima D. et al 2005 Plasma Physics and Controlled Fusion **47** 89-115
[6]. Urano H. et al 2008 Nucl. Fusion **48** 085007
[7]. Tala T. et al 2009 Physical Review Letters **102** 175002
[8]. Mantica P. et al 2009 Physical Review Letters **102** 175002
[9]. Garbet X. et al 2004 Plasma Physics and Controlled Fusion **46** B557
[10]. de Vries P.C. et al 2008 Plasma Physics and Controlled Fusion **48** 065006
[11]. Yoshida M. et al 2009 Nuclear Fusion **49** 115028
[12]. Peeters A.G. et al 2007 Physical Review Letters **98** 265003

[13]. de Vries P.C. et al 2010 Plasma Physics and Controlled Fusion **52** 065004
[14]. Zastrow K-D et al 1998 Nuclear Fusion **38** 257
[15]. Sun Y. et al 2010 Plasma Physics and Controlled Fusion **52** 105007
[16]. Versloot T.W. et al 2010 Plasma Physics and Controlled Fusion **52** 045014
[17]. Peeters A.G. et al 1998 Plasma Physics and Controlled Fusion **40** 703-706
[18]. Mahdavi et el 2003 Physics of Plasmas **10** 3984
[19]. Owen L.W. et al 1998 Plasma Physics and Controlled Fusion, **40**, p717
[20]. Carreras B.A. et al 1998 Physics of Plasmas **5** 2623
[21]. Hazeltine R.D. et al 1992 Nuclear Fusion, **32**, 3-14
[22]. Stacey W.M. 2010 Physics of Plasmas **17**, 052504
[23]. Friis Z.W. et al 2010 Physics of Plasmas, **17**, 022507
[24]. Nakashima Y. et al 2008 Journal of Physics: Conference Series 123 012029
[25]. Owen L.W. et al 2010 Nuclear Fusion **50** 064017
[26]. Tunklev M. et al 1999 Plasma Physics and Controlled Fusion, **41**, 985-1004
[27]. Giroud C. et al 2008 Review of Scientific Instruments **79** 10F525
[28]. Maddison G. et al 2010 Proc. 19th PSI Conference, San Diego, O-23
[29]. Bolvin R.L. et al 2000 Physics of Plasmas **7** 1919
[30]. Horton L.D. 2000 Plasma Physics and Controlled Fusion, **42**, A37
[31]. Tendler M. et al 1987 Fusion Technology **11** 289-310
[32]. Carreras B.A. et al 1996 Physics of Plasmas, **3** 11 4106-4114
[33]. Tomar S. 1981 Journal of Computational Physics **40** 104-119
[34]. Valovic M. et al 2004 Plasma Physics and Controlled Fusion **46** 1877-1889
[35]. Moulton D. et al 2010 Proc. 19th PSI Conference, San Diego, P3-75
[36]. Callen J.D. et al 2010 Nuclear Fusion **50** 064004
[37]. Heikinnen J.A. et al 1995 Physics of Plasmas, **2** 3724-3733
[38]. Saibene G. et al 2002 Plasma Physics and Controlled Fusion **44** 1769

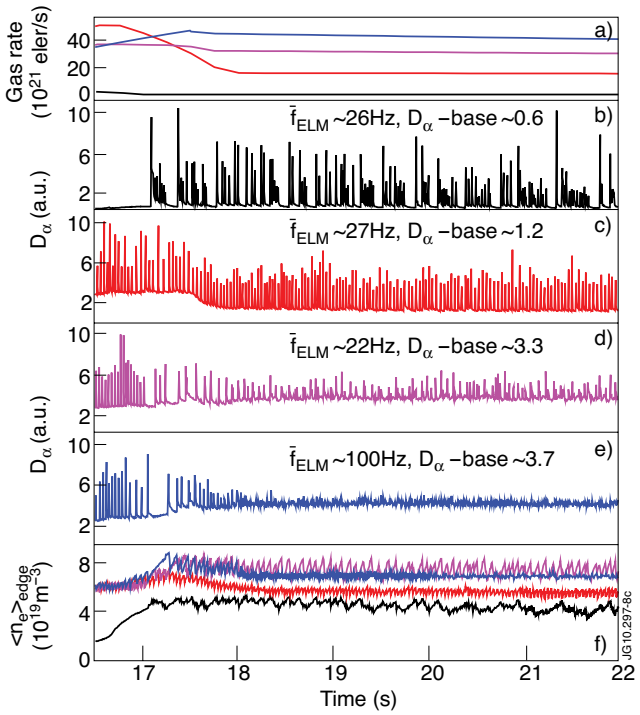

Figure 1: Time traces for several discharges at increasing external gas supply with (a) external gas rate (b-e) Corresponding D_α-emission (vertical outboard line of sight) and time-average ELM frequency (f) edge line averaged density. Notice the increase in baseline emission due to the increased neutral background in combination with a higher electron density. In general, a transition from large ELMs to small and a high frequency ELM is observed.

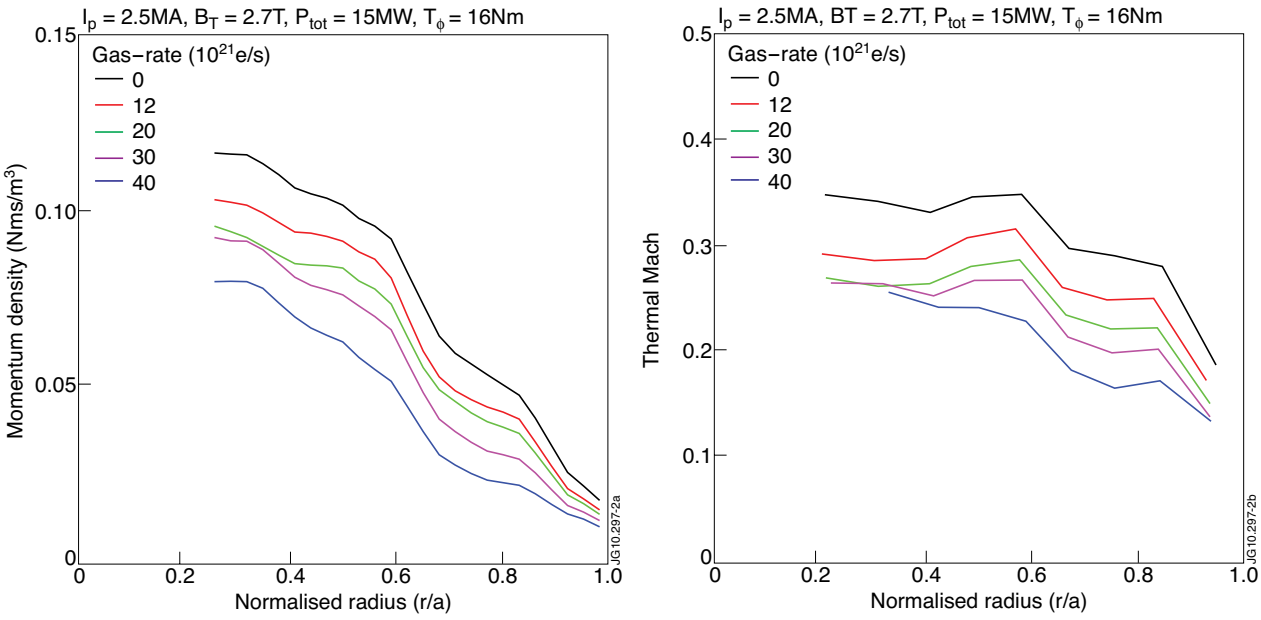

Figure 2: ELM-averaged momentum density (a) and thermal Mach (b) profile for increasing external gas dosing (see also Figure 1). A global decrease in momentum density despite an increase in ion density. Notice the large decrease in thermal Mach number at the outer radius.

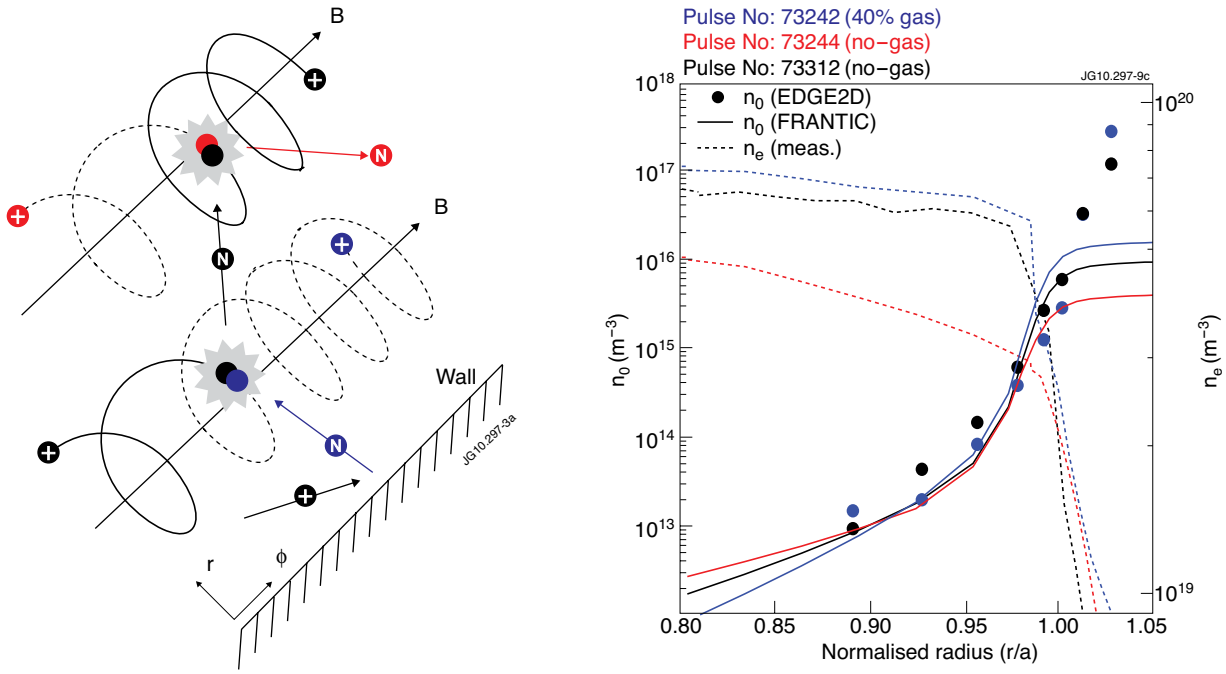

Figure 3: (left) Neutral (n_0) and electron (ne) density profiles for both non-fuelled and maximum fuelled discharges. For comparison, the calculated neutral densities from a 2D simulation code (EDGE2D-EIRENE) are over plotted. An agreement in the order of magnitude with the 1.5D neutral transport response is obtained after adjustment with the PCX method. (right) Schematic representation of a multiple charge-exchange interaction process.

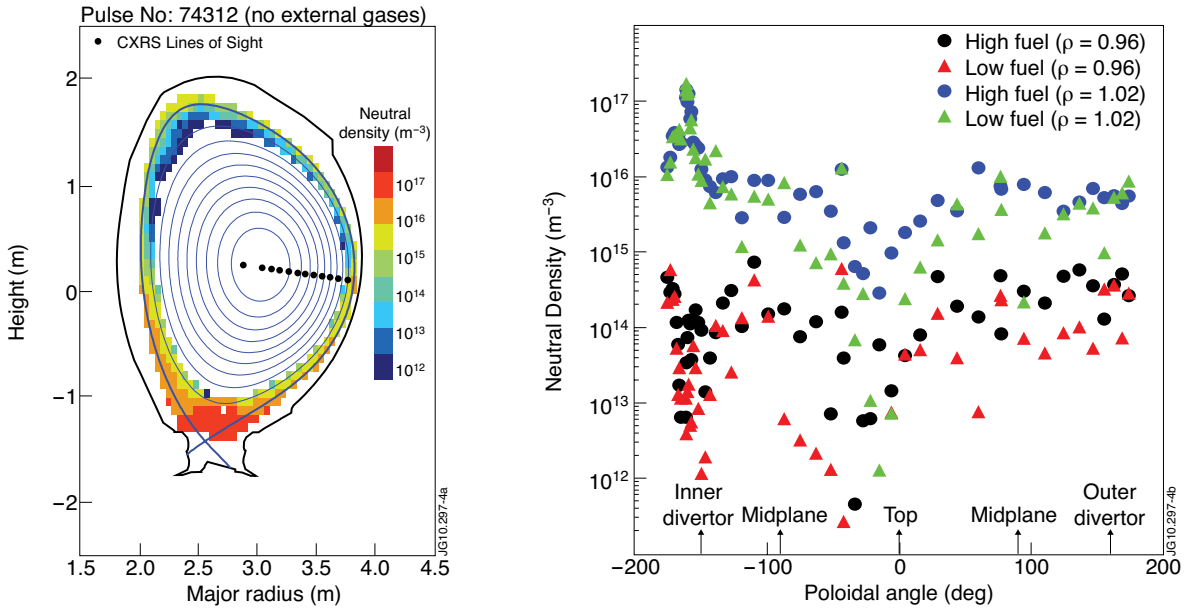

Figure 4: (left) 2D neutral density profile from EDGE2D-EIRENE for a typical non-fuelled case (see [31]). (right) Neutral density as a function of poloidal angle for both a high-fuelled and low-fuelled case. Locations just within and just outside the separatrix are shown. Notice the order of magnitude poloidal variations. The neutral density is highest near the X-point region, but drop off quickly due to fieldline flux expansion.

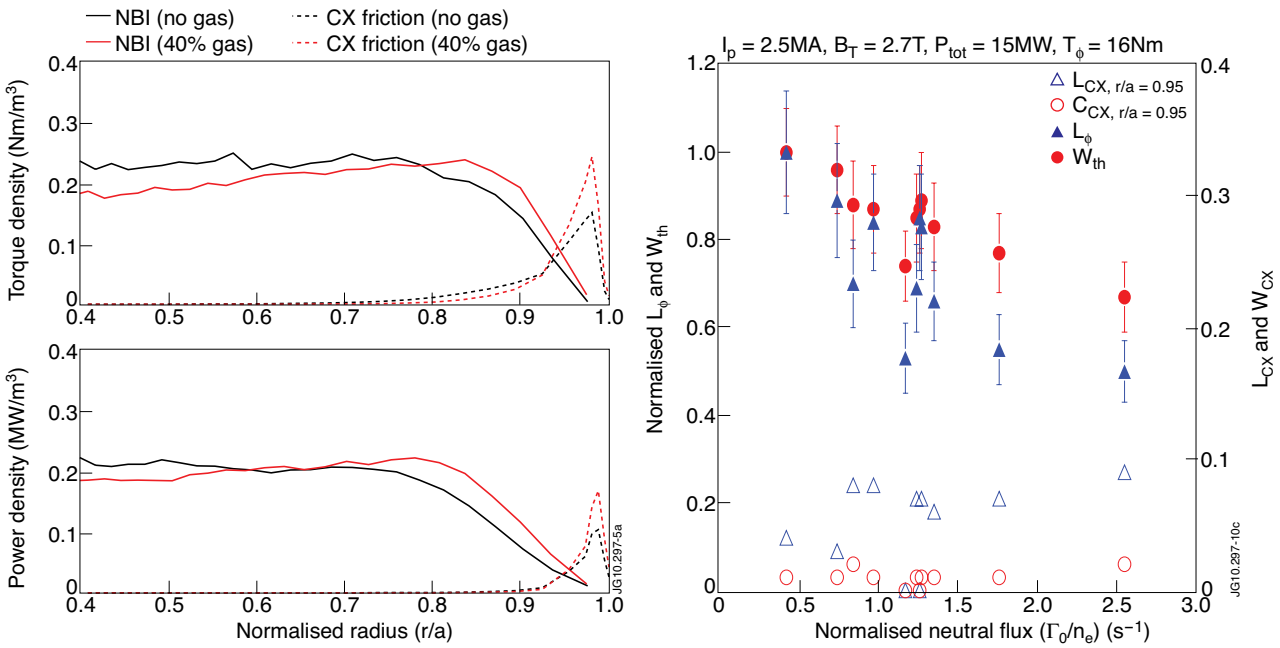

Figure 5: (a) Beam torque (top) and power (bottom) deposition profile calculated by ASCOT and charge-exchange friction components (shown positively) (b) W_{th} (circles) and L_{ϕ} (triangles) normalised to a reference discharge without external fuelling. Open symbols refer to the charge-exchange losses using the calibrated neutral density profile and integrated up to r/a~0.95 of the plasma radius.

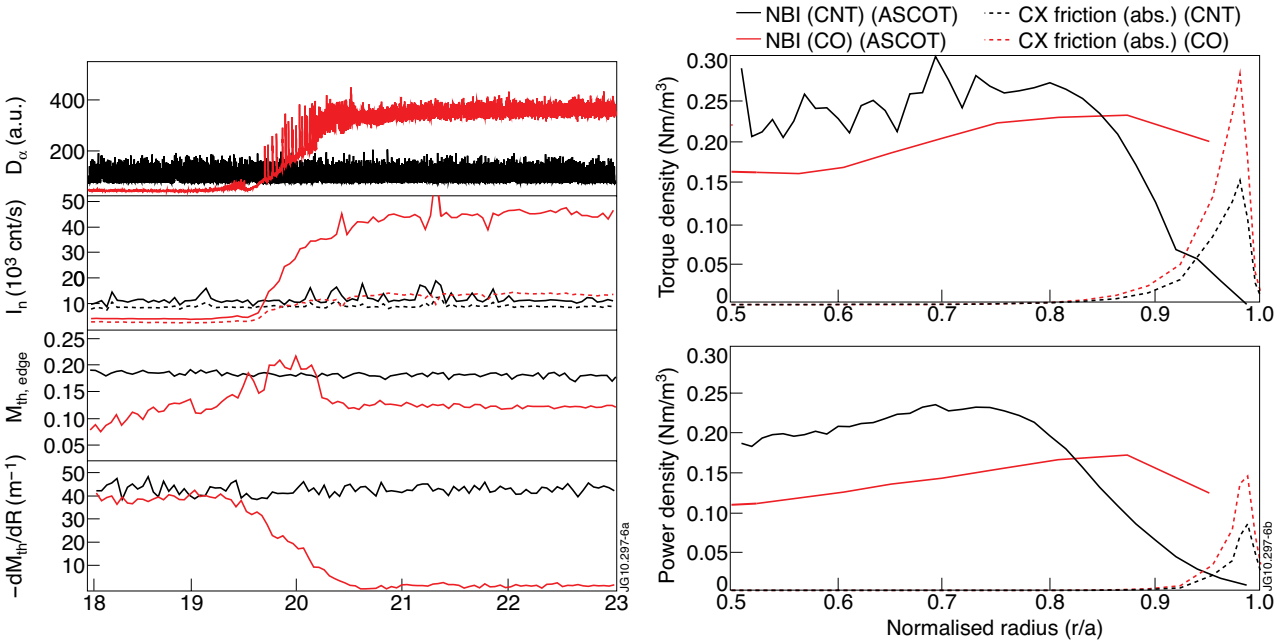

Figure 6: Comparison of co-current (CO) and counter-current (CNT) NBI discharges at similar input conditions. (a) Time trace of D_{α}-emission, the $n_{0,cold}$ and $n_{0,hot}$ signal intensity from Dα-spectrum, the edge M_{th} and the gradient of the M_{th} profile at mid-radius [r/a~0.4-0.7]. (b) Beam torque deposition profile (calculated with ASCOT) and charge-exchange friction (shown as positive) (top) and power deposition and losses (bottom). Notice the outward shift in beam torque due to prompt orbit losses and increased charge-exchange friction in the case of counter-current NBI.

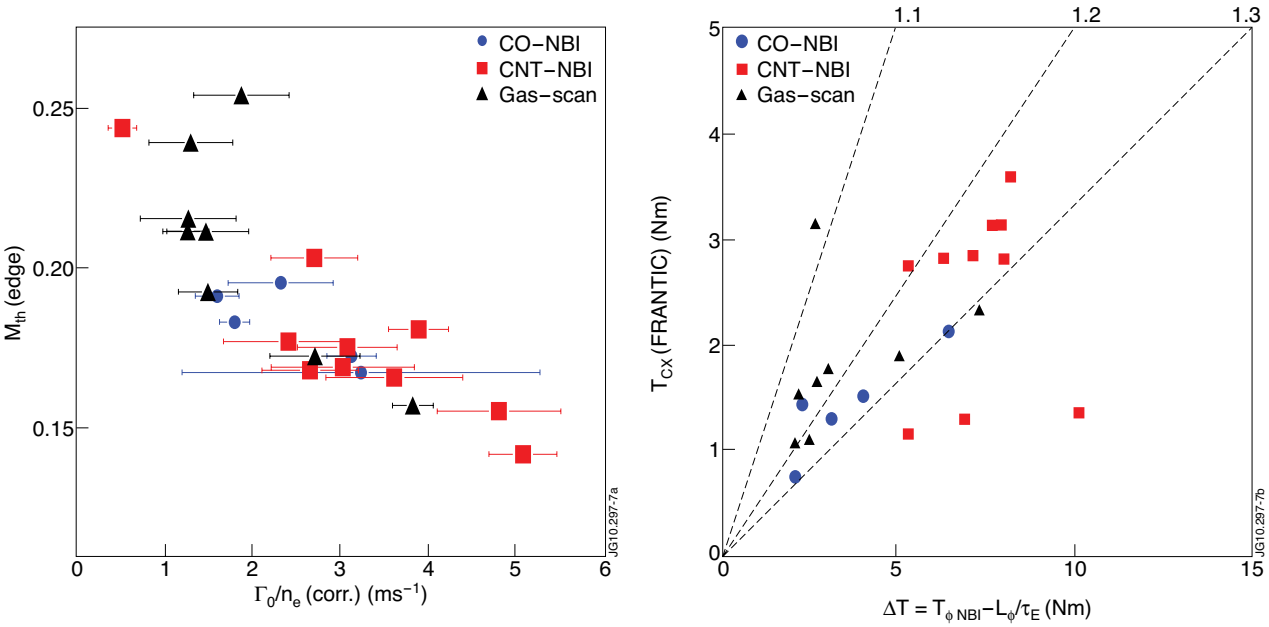

Figure 7: (left) Thermal Mach at the plasma edge (r/a~0.9) as a function of normalised neutral influx. (right) Friction torque using FRANTIC with PCX correction versus approximation of global loss torque required when assuming $\tau_E \sim \tau_\phi$. Both contribution are of similar order. Also notice the large frictional drag in the counter-current cases. Prompt first orbit losses and the increased wall interaction cause a significant increase in neutral influx.